A three-layer eight-octant phase mask towards broadband high-contrast observations

Naoshi Murakami*[a], Jun Nishikawa[b,c,d], Natsumi Akaiwa[e], Yusuke Komuro[e], Naoshi Baba[f], Motohide Tamura[b,d,g]

[a]Division of Applied Physics, Faculty of Engineering, Hokkaido University, Kita-13, Nishi-8, Kita-ku, Sapporo, Hokkaido 060-8628, Japan; [b]Extrasolar Planet Detection Project Office, National Astronomical Observatory of Japan, 2-21-1, Osawa, Mitaka, Tokyo 181-8588, Japan; [c]School of Physical Sciences, The Graduate University for Advanced Studies, 2-21-1, Osawa, Mitaka, Tokyo 181-8588, Japan; [d]AstroBiology Center, National Institutes of Natural Sciences, 2-21-1, Osawa, Mitaka, Tokyo 181-8588, Japan; [e]Department of Applied Physics, Graduate School of Engineering, Hokkaido University, Kita-13, Nishi-8, Kita-ku, Sapporo, Hokkaido 060-8628, Japan; [f]Muroran Institute of Technology, 27-1, Mizumoto-cho, Muroran, Hokkaido 050-8585, Japan; [g]Department of Astronomy, The University of Tokyo, 7-3-1, Hongo, Bunkyo-ku, Tokyo 113-0033, Japan

ABSTRACT

We designed and fabricated an achromatic eight-octant phase mask (8OPM) for broadband coronagraphic observations of exoplanets. The 8OPM is composed of three-layer eight-octant half-wave plates based on photonic crystals. By using Jones calculus, it is shown that the three-layer 8OPM achieves much higher contrast over broad wavelength range than that of the previous single-layer design. We carry out preliminary laboratory experiments of the coronagraph using the fabricated three-layer 8OPM. As a model star, we use several visible laser light sources for characterizing the coronagraphic performance. As a result, we obtain higher contrasts than theoretical ones of the single-layer 8OPM. However, the achieved contrasts are lower than the theoretical values of the three-layer one. At present we suspect that fabrication errors of the half-wave plates in the 8OPM limit the achieved contrasts.

Keywords: high-contrast imaging, coronagraph, eight-octant phase mask, exoplanets, photonic crystal

1. INTRODUCTION

More than 3000 exoplanets have been discovered since the first discovery in 1995[1]. In recent years, several tens of giant planets including possible ones (e.g., Fomalhaut b, HR8799 b,c,d,e, β Pic b, GJ504 b, and so on) have been directly imaged[2-5] . For the direct imaging of the exoplanets, high-contrast instruments are required to strongly eliminate bright starlight. For example, a 10^{-10} contrast would be necessary at an angular separation of 0.1 arcsec from a host star for directly imaging an Earth-like exoplanet at a habitable zone around a Sun-like star located at 10 pc from us.

Many advanced concepts for the high-contrast observations have been proposed and developed to date. It would be worth mentioning that direct imaging of the Earth-twin has been successfully demonstrated in a laboratory using a band-limited coronagraph[6]. The phase-mask coronagraphs, such as a four-quadrant phase-mask (4QPM), eight-octant phase-mask (8OPM), and optical (or vector) vortex coronagraphs, are also some of attracting concepts[7-10]. Several kinds of the coronagraphic phase masks have been installed into the ground-based telescopes for conducting on-sky high-contrast observations[11-14]. The vortex coronagraph[9,10], as well as the phase-induced amplitude apodization (PIAA) coronagraph[15], has an ideal observational capability in terms of the useful throughput. The vortex coronagraph has a small inner-working angle (IWA), high optical throughput, and a full 360° field of view on sky. The segmented phase-mask (4QPM, 8OPM, and also 4N-segmented phase masks[16]) coronagraphs, on the other hand, have similar observational capabilities except for the on-sky field of view, because the segmented phase-mask coronagraphs have on-sky observational "dead

*nmurakami@eng.hokudai.ac.jp; phone 81 11 706-6720; fax 81 11 706-7811

Advances in Optical and Mechanical Technologies for Telescopes and Instrumentation II, edited by Ramón Navarro, James H. Burge, Proc. of SPIE Vol. 9912, 99126G
 · doi: 10.1117/12.2231946

zones" along phase transitions of the masks. However the on-sky dead zones can be avoided by rotating the phase mask by 45° for the 4QPM or 22.5° for the 8OPM. We expect that the segmented phase-mask coronagraphs would also be attracting tools for direct imaging of exoplanets thanks to their simple mask designs with binary structures.

Recently coronagraphic phase masks based on photonic-crystal technology have been proposed. The photonic crystals, artificial periodic nanostructures of high and low refractive indices, would be advantageous for the coronagraphic phase masks owing to its extremely small fabrication defects. The 8OPM and the vortex phase masks have been fabricated based on the photonic crystals[17,18]. These masks are composed of space-variant half-wave plates (HWPs), that is, HWPs with space-variant fast axes. Phase shifts required for the coronagraphic masks are realized by making use of the Pancharatnam-Berry phase[19,20], which depends on orientation angles of the fast axes of the space-variant HWPs. For example, the orientation angles have to be set to ±45° alternately in eight-octant sectors for realizing the $0/\pi$ phase modulation required for the 8OPM. However, it would be difficult to realize achromatic coronagraphic devices because the photonic-crystal HWPs exhibit chromatic characteristics and their phase retardations depend on a wavelength. In other words, extremely high-contrast observations are realized only at an optimized wavelength of the coronagraphic mask. For realizing broadband high-contrast observations, polarization-filtered photonic-crystal coronagraphic masks have been studied[17,18,21]. However, the polarizing filters cause additional wavefront aberrations, resulting in degradation of an achievable contrast. Furthermore, optical throughput of the coronagraphic system for planetary light would degrade due to the polarization filters.

As mentioned in the previous publication, three-layer HWPs would be an interesting solution for achromatizing the photonic-crystal 8OPM[21]. It should be noted that the application of the three-layer achromatic HWPs to the coronagraphic devices has been originally proposed in a context of the vector vortex coronagraph[22]. Compared to the original single-layer design, it is expected that an extremely high contrast can theoretically be achieved over a broad wavelength range by the three-layer 8OPM without loss of the optical throughput due to the polarization filters. As an important step, we recently fabricated a first-trial three-layer 8OPM based on the photonic-crystal technology.

Here we report our recent activity of the fabricated three-layer photonic-crystal 8OPM. We carry out preliminary laboratory experiments of the three-layer 8OPM using visible light sources to evaluate the achievable contrast. First, we show a principle of the 8OPM coronagraph in Sect. 2. Also in Sect. 2, we describe operations of polarized light passing through the single-layer and the three-layer phonic-crystal 8OPMs. Expected contrasts of the 8OPM coronagraph (both the single-layer and the three-layer masks) are derived by Jones calculus. The results of the Jones calculus are shown in Sect. 2. Preliminary laboratory experiments of the 8OPM coronagraph are reported in Sect. 3, and finally our conclusion is summarized in Sect. 4.

2. PRINCIPLE

2.1 Eight-octant phase-mask coronagraph

Figure 1 shows an optical setup of the eight-octant phase-mask (8OPM) coronagraph. Here we assume a clear circular telescope pupil in an entrance pupil plane (*a*). A lens L1 forms a stellar image in a telescope focal plane (*b*). The stellar image becomes an Airy pattern if the star is assumed to be a point-like light source. The 8OPM is placed in the telescope focal plane. In Figure 1, a phase map provided by the ideal 8OPM is also shown. In a reimaged pupil plane (*c*), a lens L2 creates a petal-like intensity pattern, and stellar light is totally diffracted outside the pupil area. Thus a perfect stellar rejection is theoretically realized by blocking the diffracted light with a Lyot stop placed in the plane (*c*). Finally exoplanetary light is directly detected in a focal plane (*d*) formed by a lens L3.

It is important to fabricate an achromatic 8OPM for broadband high-contrast observations and spectroscopic measurements of exoplanets. The photonic-crystal technology would be one of attracting approaches for the achromatic 8OPM[17]. The photonic-crystal 8OPM is composed of eight-octant half-wave plates (HWPs) with fast (or slow) axes of ±45° as shown in Figure 2. The desired phase map of the 8OPM is realized by making use of the Pancharatnam-Berry phase[19,20]. However, phase retardations of the HWPs generally depend on a wavelength of light. Polarization filtering have been proposed for reducing the effect of the wavelength-dependent phase retardation of the space-variant HWPs[23]. For the polarization filtering, two crossed (0° and 90°) linear polarizers are placed in front of and behind the photonic-crystal 8OPM. Laboratory demonstrations of the polarization-filtered 8OPM using broadband light sources have been reported[17,21,24]. Drawback of the polarization filtering is, however, its low optical throughput. Half of the planetary light

would be lost by the first polarizer if the incoming planetary light is unpolarized. In addition, an error of the phase retardation of the HWPs also causes a loss of the optical throughput at the second polarizer[17].

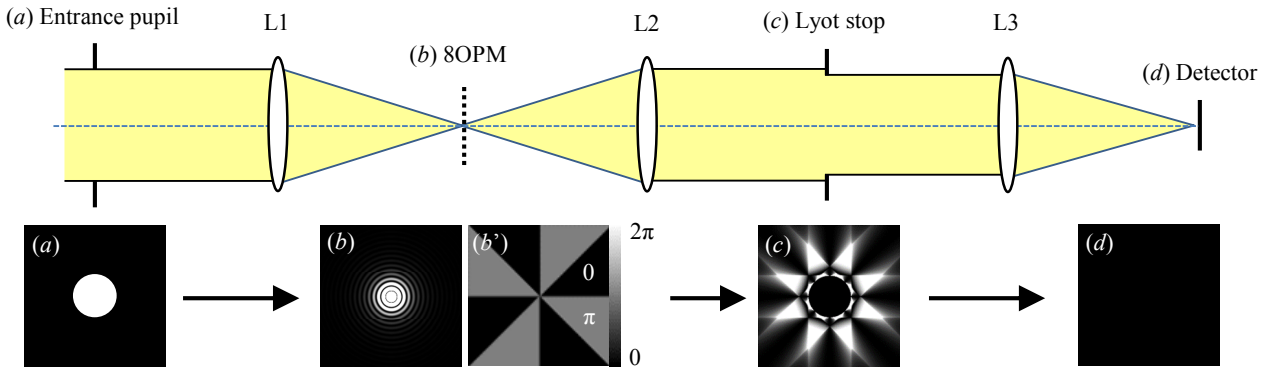

Figure 1. An optical setup of the 8OPM coronagraph. Images in four key planes as well as a phase map of the 8OPM are also shown.

For realizing the achromatic 8OPM without the polarization filtering, three-layer HWPs would be an interesting approach[21,22]. Figure 2(*c*) shows schematic design of the three-layer 8OPM. The HWP with an axis of 45° of the single-layer 8OPM is replaced with the three-layer ones with axes of 75°, 15°-δ, and 75°, while that with an axis of -45° of the single-layer 8OPM is replaced with the three-layer ones with axes of -15°, -75°-δ, and -15°. The angle δ is a design parameter described below. In Figure 2, we call four sectors shown in white "area A" while those shown in gray "area B" in the following discussions.

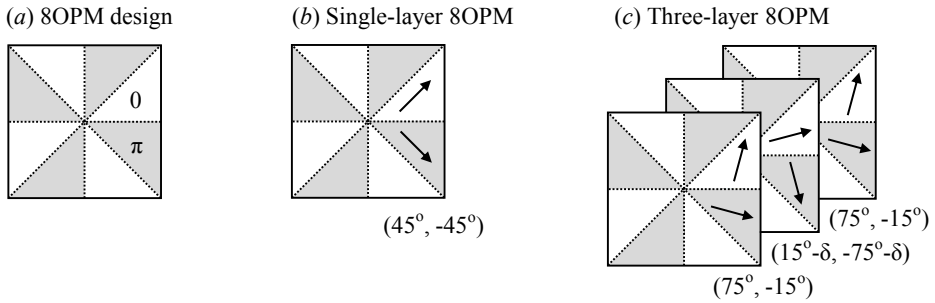

Figure 2. (*a*) A phase map of the 8OPM, (*b*) schematic design of a single-layer 8OPM, and (*c*) a three-layer 8OPM.

2.2 Design and operation of three-layer 8OPM

Here we show an operation of the 8OPM based on Jones calculus. As shown in Figure 3(*a*), we assume that x-polarized light, described by a Jones vector $\boldsymbol{E}_{ix}$, is incoming to the 8OPM. A state of polarization is changed by the 8OPM according to the retardation and the fast axes of the HWPs. Then, Jones vectors of the output lights passing through the areas A and B ($\boldsymbol{E}_{oax}$ and $\boldsymbol{E}_{obx}$, respectively) are calculated by using Jones matrices of the HWPs shown in Figure 2(*b*) for the single-layer 8OPM or in Figure 2(*c*) for the three-layer 8OPM. Now we use the following Jones vector as the incoming x-polarized light:

$$\boldsymbol{E}_{ix} = E_{ix}\begin{bmatrix}1\\0\end{bmatrix}. \tag{1}$$

The subscript "*ix*" indicates the "incoming x-polarized light". Then, states of polarization of the output lights passing through the areas A and B are, respectively, written as

$$\boldsymbol{E}_{oax} = E_{oaxx}\begin{bmatrix}1\\0\end{bmatrix} + E_{oaxy}\begin{bmatrix}0\\1\end{bmatrix} \tag{2}$$

$$\boldsymbol{E}_{obx} = E_{obxx}\begin{bmatrix}1\\0\end{bmatrix} + E_{obxy}\begin{bmatrix}0\\1\end{bmatrix}. \tag{3}$$

The subscripts of the vectors "*oax*" and "*obx*" indicate the "output light passing through the area A (or B) for the incoming x-polarized light". The fourth subscripts "*x*" and "*y*" of the complex values indicate the "x-polarized and the y-polarized components", respectively.

Now we focus on the x-polarized output passing through the areas A and B whose complex amplitudes are E_{oaxx} and E_{obxx}, respectively. These electric fields are interfered in the reimaged pupil plane. Then these electric fields can be expressed by using two complex values: in-phase and out-of-phase components as:

$$E_{oaxx} = E_{bright,xx} + E_{null,xx} \tag{4}$$

$$E_{obxx} = E_{bright,xx} - E_{null,xx} \tag{5}$$

These two components contribute to constructive (bright) and destructive (nulled) interferences, respectively. The electric fields corresponding to the bright and nulled components are given by

$$E_{bright,xx} = \frac{(a_{rxx} + b_{rxx}) + i(a_{ixx} + b_{ixx})}{2} \tag{6}$$

$$E_{null,xx} = \frac{(a_{rxx} - b_{rxx}) + i(a_{ixx} - b_{ixx})}{2}, \tag{7}$$

where a_{rxx}, b_{rxx}, a_{ixx}, and b_{ixx} are real and imaginary parts of the complex values E_{oaxx} and E_{obxx}, respectively. Similarly, the output y-polarized electric fields E_{oaxy} and E_{obxy} are also expressed by the bright and the nulled components $E_{bright,xy}$ and $E_{null,xy}$.

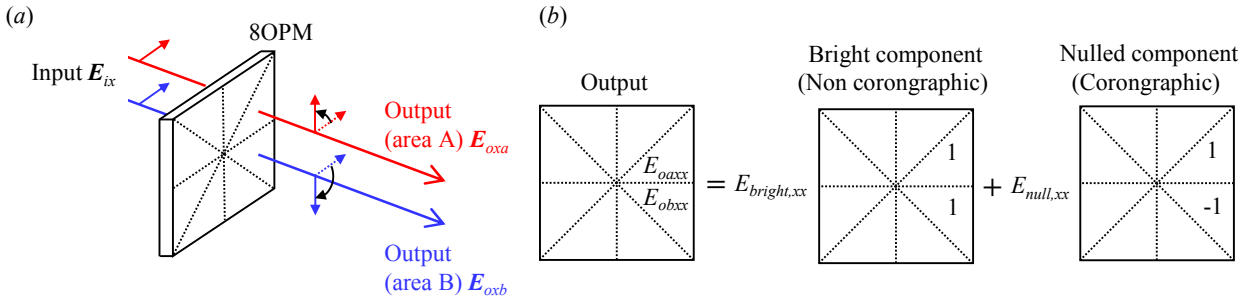

Figure 3. (*a*) A schematic illustration of a polarized light beams incoming to two areas (A and B) of the 8OPM, and (*b*) resultant complex amplitude of the 8OPM which can be divided into bright and nulled components.

As illustrated in Figure 3(*b*), the nulled component corresponds to the ideal 8OPM, while the bright component corresponds to a situation without a coronagraphic mask in the focal plane. Theoretically the nulled component creates the petal-like pattern in the reimaged pupil plane, and realizes perfect stellar rejection for a point-like star in the final focal plane. On the other hand, the bright component creates the clear circular beam similar to the entrance pupil, whose amplitude is reduced by a factor of $|E_{bright,xx}|/|E_{ix}|$. Similarly, the bright and nulled components $E_{bright,xy}$ and $E_{null,xy}$ can be

calculated for the y-polarized outputs E_{oaxy} and E_{obxy} in Eqs. (2) and (3). Finally, the achievable contrast of the 8OPM coronagraph for the x-polarized input would be estimated as the following equation.

$$C_x = \frac{\left|E_{bright,xx}\right|^2 + \left|E_{bright,xy}\right|^2}{\left|E_{ix}\right|^2}. \tag{8}$$

We note that the incoming unpolarized (or partially polarized) light is expressed as an incoherent (or partially coherent) sum of the x- and y-polarized lights. The contrast for the y-polarized input can also be estimated in the same way.

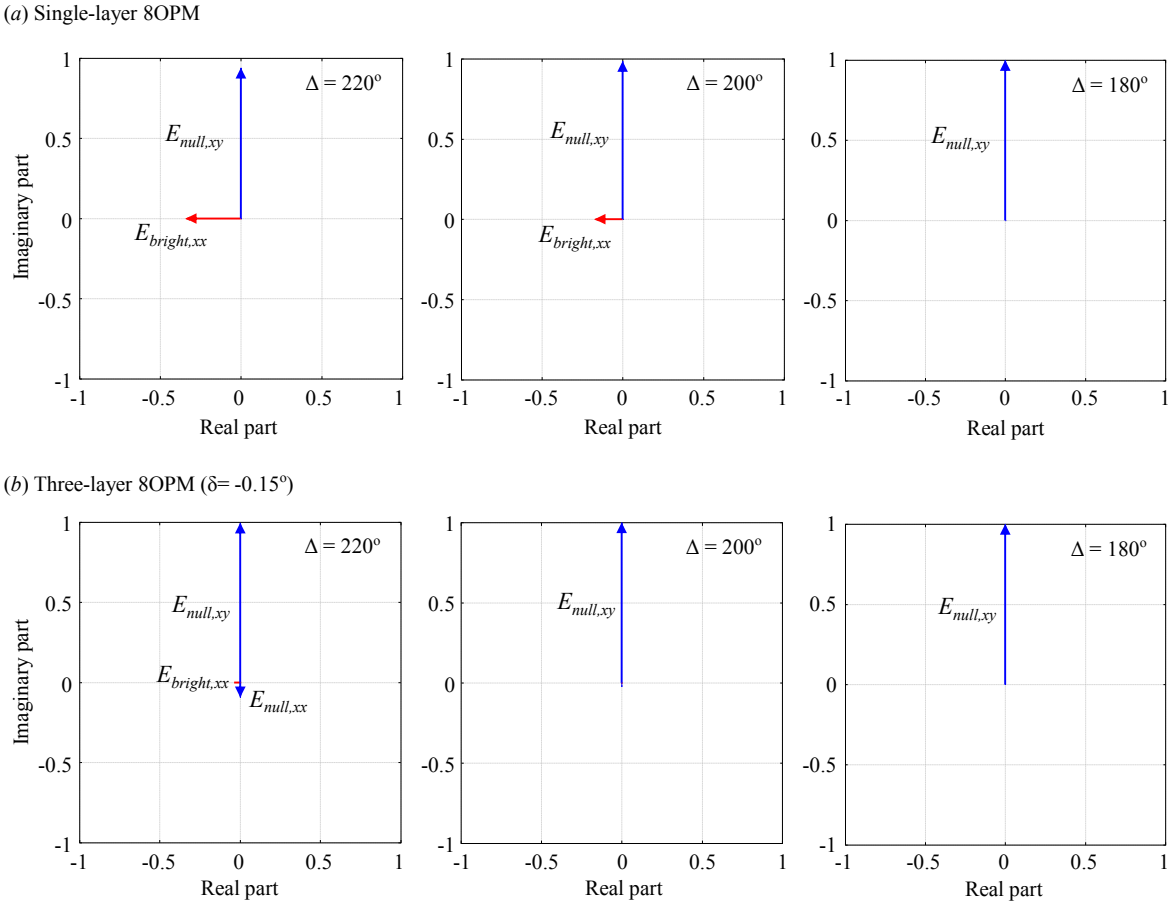

Figure 4. Calculated bright and nulled components as vectors in complex planes for (*a*) the single-layer and (*b*) the three-layer 8OPMs. The three examples, assuming that ideal HWPs (Δ=180°) and imperfect HWPs (Δ=200° and 220°) are used for the 8OPM, are shown.

Figure 4 shows calculated bright and nulled components as vectors in complex planes for (*a*) the single-layer and (*b*) the three-layer 8OPMs. We show results of three examples assuming that ideal HWPs (the phase retardation of Δ = 180°) and imperfect HWPs (phase retardations of Δ = 200° and 220°) are used for the 8OPM. In the ideal case (Δ = 180°), only the nulled components $E_{null,xy}$ appear in the complex planes for the both single-layer and the three-layer 8OPMs, which suggests that the perfect stellar elimination is theoretically realized by both mask designs if the ideal HWPs are used for the 8OPMs. We note that the nulled component $E_{null,xy}$ is y-polarized as illustrated in Figure 3(*a*).

In the imperfect cases of Δ=200° and Δ=220°, not only the nulled component $E_{null,xy}$ but also the bright component $E_{bright,xx}$ appear in the result of the single-layer 8OPM. The bright component of the output light is x-polarized one, which is parallel to the input polarization. Thus, the unwanted bright component can be blocked by using a 90° linear polarizer behind the 8OPM. This is why the polarization filtering (crossed polarizers) is useful for achromatizing the single-layer 8OPM. For the single-layer 8OPM, the bright component becomes larger as an error of the phase retardation increases. For the three-layer 8OPM, on the other hand, the bright component is still very small even in the case of the large retardation error (Δ = 220°). Therefore, it is expected that the three-layer 8OPM achieves very high contrast even at wavelengths where the HWPs are not optimized.

In Figure 5, we show estimated contrasts as a function of the phase retardation Δ for the single-layer and the three-layer 8OPMs calculated by Eq. (8). For the three-layer 8OPM, we assume two design parameters (δ = -0.15° and -0.5°). When the 8OPMs are composed of ideal HWPs (Δ = 180°), both the single-layer and the three-layer 8OPMs provide perfect stellar rejection (C = 0). When the phase retardation is Δ = 0° and 360°, on the other hand, we can see that the 8OPM cannot reject starlight at all (the estimated contrast becomes unity, C = 1). This is because a state of polarization of the incoming light cannot be changed by the 8OPM at these phase retardations corresponding to a situation without any coronagraphic mask in the focal plane.

Figure 5 demonstrates that the three-layer 8OPMs realize much higher contrast than that of the single-layer one over a broad range of the phase retardation. Thus it is expected that broadband high-contrast observations are feasible by using the three-layer 8OPM. We note that the design parameter δ adjusts an achievable contrast and an effective bandwidth as demonstrated.

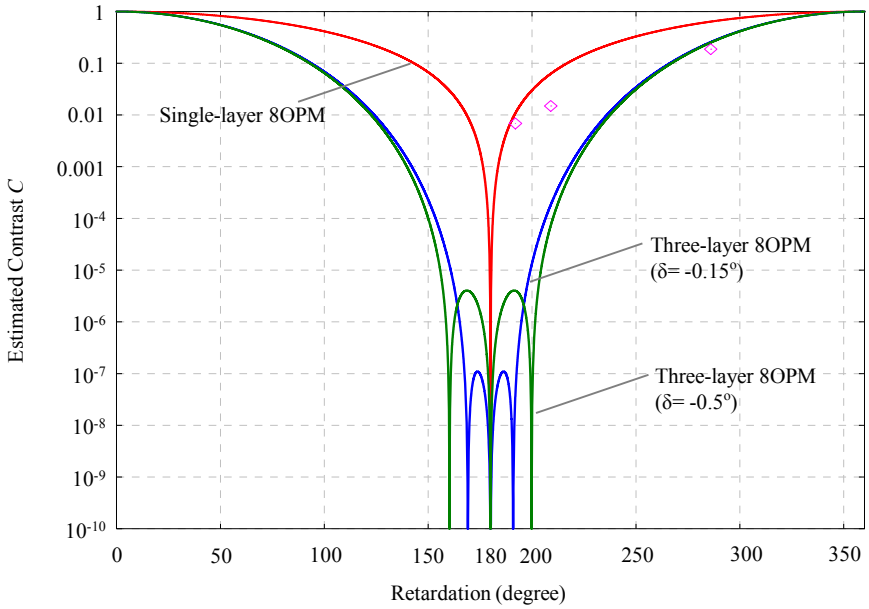

Figure 5. Estimated contrasts as a function of a phase retardation Δ of the 8OPM. Three curves are the estimated contrasts assuming the single-layer 8OPM and the three-layer one with the design parameter δ=-0.15° and -0.5°. Three plots are results of the laboratory experiments using three monochromatic laser light sources.

3. PRELIMINARY LABORATORY EXPERIMENTS

The three-layer 8OPM is fabricated based on the photonic-crystal technology. The photonic-crystal technology, so-called the autocloning technique (the Photonic Lattice, Inc.)[25-26], has been utilized for fabricating the single-layer space-variant HWPs for the 8OPMs and the vortex phase masks[17-18]. These single-layer coronagraphic masks are composed of photonic-crystal layers formed on substrates. The first-trial three-layer 8OPM is, on the other hand, composed of the first

and the second layers on a front side and the third layer on a back side of a substrate with a thickness of 0.5 mm. An effective area of the 8OPM part is 5×5 mm^2, and the design parameter is set to $\delta = -0.15°$.

We carry out preliminary laboratory experiments of the 8OPM coronagraph using the three-layer device. Figure 6 shows an optical setup of the laboratory experiments. As a model star, we use three laser light sources with wavelengths of λ = 532, 633, and 670 nm. We place a small circular aperture with a diameter of D = 1.5 mm in a collimated beam for simulating a telescope pupil. The model star is imaged in a focal plane with an F/100 converging beam. For these optical parameters, the effective area of the 8OPM corresponds to about 94×94, 79×79, and 75×75 λ/D for the wavelengths λ = 532, 633, and 670 nm, respectively. In Figure 6, a picture of the first-trial three-layer 8OPM mounted on a rotatable holder is also shown.

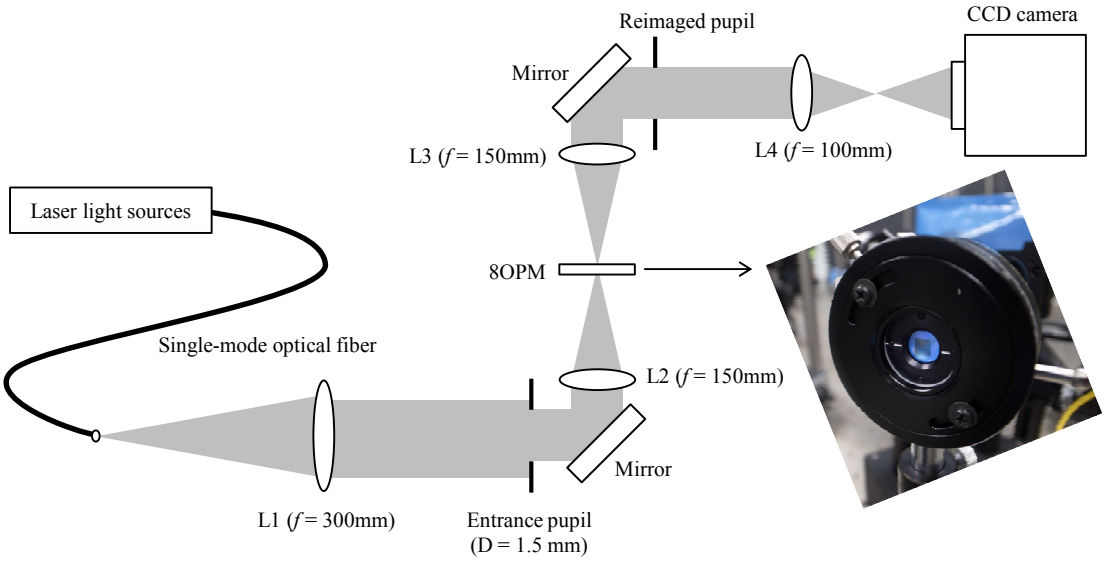

Figure 6. An optical setup of a laboratory demonstration and a picture of the fabricated three-layer 8OPM mounted on a rotatable holder.

Figure 7 shows acquired images, with the light sources (*a*) λ = 532 nm, (*b*) 633 nm and (*c*) 670 nm, in the reimaged pupil plane where a Lyot stop should be placed. The first-trial three-layer 8OPM is optimized at a wavelength of roughly 700 nm, so the experimental result at λ = 670 nm is most similar to a numerically simulated image, shown in Figure 7(*d*), assuming an ideal 8OPM.

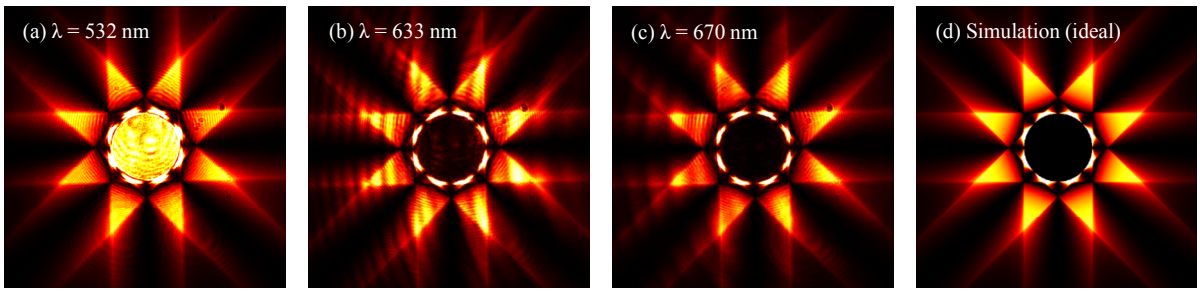

Figure 7. Results of preliminary laboratory demonstration. The images are acquired in the reimaged pupil plane using monochromatic laser light sources with wavelengths of (*a*) 532 nm, (*b*) 633 nm, and (*c*) 670 nm. The numerically simulated images assuming an ideal 8OPM is also shown (*d*).

For estimating the contrast, we calculate the following value:

$$C_{meas} = \frac{\int_{incide} I(x,y)dxdy}{\int_{total} I(x,y)dxdy}, \tag{9}$$

where $I(x, y)$ is an acquired image in the reimaged pupil plane (x, y). The integrations are calculated over a whole region for the denominator, while calculated over only a circular pupil area for the numerator. By using Eq. (9), we calculate the contrasts $C_{meas} = 1.9\times10^{-1}$, 1.5×10^{-2}, and 6.9×10^{-3} for the wavelengths of $\lambda = 532$, 633, and 670 nm, respectively.

In Figure 5, we plot the experimentally obtained contrasts C_{meas} for the three wavelengths. The contrasts obtained by the first-trial three-layer 8OPM are somehow better than the theoretically estimated contrast of the single-layer 8OPM, but worse than that of the three-layer 8OPM. At present we suspect that fabrication errors of the first-trial device (e.g., difference in phase retardations between the layers) limit the experimentally obtained contrast. In future we will have to carry out laboratory experiments of the coronagraph using a white light source with various bandpass filters to obtain more data at additional wavelengths. These experimental data will be useful for characterizing the fabrication errors of the 8OPM.

4. CONCLUSION

We reported our recent activity of the three-layer photonic-crystal 8OPM for broadband high-contrast observations. First we derived the output electric fields of the three-layer 8OPM based on the Jones calculus, and demonstrated that the output electric fields are mathematically expressed by a sum of the bright (non-coronagraphic) and nulled (coronagraphic) components. The achievable contrast of the 8OPM coronagraph with the three-layer device has also been estimated from the Jones calculus. We fabricated the first-trial three-layer 8OPM based on the photonic-crystal technology. As a result of the laboratory demonstrations, the achieved contrasts were worse than the theoretical ones at present. We suspect that the fabrication errors of the 8OPM limit the experimentally obtained contrast. Toward a second-trial device with better performance, we are now trying to characterize the fabrication errors by comparing laboratory experiments and numerical simulations. Furthermore, we have been also developing observational techniques related to the 8OPM coronagraph for enhancing the achievable contrast, such as polarimetric technique, pre-optics for reducing an effect of a central obscuration, and so on. These activities will be reported in forthcoming papers.

ACKNOWLEDGMENT

We thank Takayuki Kawashima of the Photonic Lattice Inc. for useful information on photonic-crystal devices. We also thank Kazuhiko Oka of Hokkaido University for his helpful comments on the laboratory experiments. Part of this work was achieved using the grant of Joint Development Research supported by the Research Coordination Committee, National Astronomical Observatory of Japan (NAOJ). This work was also partly supported by the Japan Society for the Promotion of Science (JSPS) through KAKENHI (26287026).

REFERENCES

[1] Mayor, M. and Queloz, D., "A Jupiter-mass companion to a solar-type star," Nature 378, 355-359 (1995).
[2] Kalas, P., Graham, J. R., Chiang, E., Fitzgerald, M. P., Clampin, M., Kite, E. S., Stapelfeldt, K., Marois, C. and Krist, J., "Optical Images of an Exosolar Planet 25 Light-Years from Earth," Science 322, 1345-1348 (2008).
[3] Marois, C., Macintosh, B., Barman, T., Zuckerman, B., Song, I., Patience, J., Lafrenière, D. and Doyon, R., "Direct imaging of multiple planets orbiting the star HR 8799," Science 322, 1348-1352 (2008).
[4] Lagrange, A.-M., Bonnefoy, M., Chauvin, G., Apai, D., Ehrenreich, D., Boccaletti, A., Gratadour, D., Rouan, D., Mouillet, D., Lacour, S. and Kasper, M., "A giant planet imaged in the disk of the young star β Pictoris," Science 329, 57-59 (2010).

[5] Kuzuhara, M., Tamura, M., Kudo, T., Janson, M., Kandori, R., Brandt, T. D., Thalmann, C., Spiegel, D., Biller, B., Carson, J., Hori, Y., Suzuki, R., Burrows, A., Henning, T., Turner, E. L., McElwain, M. W., Moro-Martín, A., Suenaga, T., Takahashi, Y. H., Kwon, J., Lucas, P., Abe, L., Brandner, W., Egner, S., Feldt, M., Fujiwara, H., Goto, M., Grady, C. A., Guyon, O., Hashimoto, J., Hayano, Y., Hayashi, M., Hayashi, S. S., Hodapp, K. W., Ishii, M., Iye, M., Knapp, G. R., Matsuo, T., Mayama, S., Miyama, S., Morino, J.-I., Nishikawa, J., Nishimura, T., Kotani, T., Kusakabe, N., Pyo, T.-S., Serabyn, E., Suto, H., Takami, M., Takato, N., Terada, H., Tomono, D., Watanabe, M., Wisniewski, J. P., Yamada, T., Takami, H. and Usuda, T., "Direct imaging of a cold Jovian exoplanet in orbit around the Sun-like star GJ 504," Astrophys. J. 774: 11 (18pp) (2013).
[6] Trauger, J. T. and Traub, W. A., "A laboratory demonstration of the capability to image an Earth-like extrasolar planet," Nature 446, 771-773 (2007).
[7] Rouan, D., Riaud, P., Boccaletti, A., Clénet, Y. and Labeyrie, A., "The four-quadrant phase-mask coronagraph. I. principle," Publ. Astron. Soc. Pacific 112, 1479-1486 (2000).
[8] Murakami, N., Uemura, R., Baba, N., Nishikawa, J., Tamura, M., Hashimoto, N. and Abe, L., "An eight-octant phase-mask coronagraph," Publ. Astron. Soc. Pacific 120, 1112-1118 (2008).
[9] Foo, G., Palacios, D. M. and Swartzlander, G. A. Jr., "Optical vortex coronagraph," Opt. Lett. 30, 3308-3310 (2005).
[10] Mawet. D., Riaud, P., Absil, O. and Surdej, J., "Annular groove phase mask coronagraph," Astrophys. J. 633, 1191-1200 (2005).
[11] Boccaletti, A., Riaud, P. and Lagrange A. -M., "The four-quadrant phase mask coronagraph. IV. First light at the Very Large Telescope," Publ. Astron. Soc. Pacific 116, 1061-1071 (2004).
[12] Swartzlander, G. A. Jr., Ford, E. L., Abdul-Malik, R. S., Close, L. M., Peters, M. A., Palacios, D. M. and Wilson, D. W., "Astronomical demonstration of an optical vortex coronagraph," Opt. Express 16, 10200-10207 (2008).
[13] Mawet, D., Serabyn, E., Liewer, K., Burruss, R., Hickey, J. and Shemo, D., "The vector vortex coronagraph: laboratory results and first light at Palomar Observatory," Astrophys. J. 709, 53-57 (2010).
[14] Serabyn, E., Mawet, D. and Burruss, R., "An image of an exoplanet separated by two diffraction beamwidths from a star," Nature 464, 1018-1020 (2010).
[15] Guyon, O., "Phase-induced amplitude apodization of telescope pupils for extrasolar terrestrial planet imaging," Astron. Astrophys. 404, 379-387 (2003).
[16] Carlotti, A., Ricort, G. and Aime, C., "Phase mask coronagraphy using a Mach-Zehender interferometer," Astron. Astrophys. 504, 663-671 (2009).
[17] Murakami, N., Nishikawa, J., Yokochi, K., Tamura, M., Baba, N. and Abe, L., "Achromatic eight-octant phase-mask coronagraph using photonic crystal," Astrophys. J. 714, 772-777 (2010).
[18] Murakami, N., Hamaguchi, S., Sakamoto, M., Fukumoto, R., Ise, A., Oka, K., Baba, N. and Tamura, M., "Design and laboratory demonstration of an achromatic vector vortex coronagraph," Opt. Express 21, 7400-7410 (2013).
[19] Pancharatnam, S., "Generalized theory of interference, and its applications," Proc. Indian Acad. Sci. 44, 247-262 (1956).
[20] Berry, M., "The adiabatic phase and Pancharatnam's phase for polarized light," J. Mod. Opt. 34, 1401-1407 (1987).
[21] Murakami, N., Nishikawa, J., Tamura, M., Serabyn, E., Traub, W. A., Liewer, K. M., Moody, D. C., Trauger, J. T., Guyon, O., Martinache, F., Jovanovic, N., Singh, G., Oshiyama, F., Shoji, H., Sakamoto, M., Hamaguchi, S., Oka, K. and Baba, N., "Recent progress on phase-mask coronagraphy based on photonic-crystal technology," Proc. SPIE 9143, 914334-1-914334-8 (2014).
[22] Mawet, D., Pueyo, L., Moody, D., Krist, J. and Serabyn, E., "The vector vortex coronagraph: sensitivity to central obscuration, low-order aberrations, chromaticism, and polarization," Proc. SPIE 7739, 773914-1-773914-13 (2010).
[23] Baba, N., Murakami, N., Ishigaki, T. and Hashimoto, N., "Polarization interferometric stellar coronagraph," Opt. Lett. 27, 1373-1375 (2002).
[24] Murakami, N., Nishikawa, J., Traub, W. A., Mawet, D., Moody, D. C., Kern, B. D., Trauger, J. T., Serabyn, E., Hamaguchi, S., Oshiyama, F., Sakamoto, M., Ise, A., Oka, K., Baba, N., Murakami, H. and Tamura, M., "Coronagraph focal-plane phase-masks based on photonic crystal technology: recent progress and observational strategy," Proc. SPIE 8442, 844205-1-844205-9 (2012).

[25] Kawakami, S., Kawashima, T. and Sato, T., "Mechanism of shape formation of three-dimensional periodic nanostructures by bias sputtering," Appl. Phys. Lett. 74, 463-465 (1999).
[26] Kawashima, T., Miura, K., Sato, T. and Kawakami, S., "Self-healing effects in the fabrication process of photonic crystals," Appl. Phys. Lett. 77, 2613-2615 (2000).